RESEARCH PAPER

Adsorption of Methotrexate onto Rosemary-Loaded Chitosan-Poly (Acrylic Acid)/MWCNTs Nanocomposite

Mohammed A. Kadhim [1]*, *Zeina M. Kadam* [2]

[1] *Department of Science, College of Basic Education, Al-Muthanna University, Samawah, Iraq*

[2] *Department of Chemistry, College of Science, Al-Qadisiyah University, Diwaniyah, Iraq*

ARTICLE INFO

Article History:
Received 12 June 2025
Accepted 07 August 2025
Published 01 October 2025

Keywords:
Adsorption
Hydrogel
MTX
MWCNTs
Rosemary

ABSTRACT

In this work, a novel rosemary-loaded chitosan-poly (acrylic acid)/multi-walled carbon nanotube (MWCNTs) nanocomposite was synthesized via free radical polymerization and employed as an efficient adsorbent for the removal of methotrexate (MTX) from aqueous solutions. The integration of rosemary provided bioactive functionality and enhanced surface characteristics. The composite was comprehensively characterized using FTIR, XRD, SEM, TEM, EDX, and zeta potential (–46.5 mV), confirming successful synthesis, porosity, and structural stability. Batch adsorption experiments revealed optimal MTX uptake at pH 4 and 90 minutes, with rapid initial adsorption and high efficiency. Kinetic modeling showed that the process followed pseudo-second-order kinetics, indicating chemisorption. Isotherm analysis revealed that the Freundlich model best described the data (K_F = 9.903, R^2 = 0.9942), suggesting multilayer adsorption on a heterogeneous surface. Thermodynamic parameters (ΔG = –2.37 kJ/mol, ΔH = –10.72 kJ/mol, ΔS = –28.5 J/mol·K) indicated that the adsorption is spontaneous and exothermic. The nanocomposite also showed partial reusability, retaining 78% adsorption efficiency after three cycles. These results highlight the potential of this eco-friendly, plant-based nanocomposite for applications in targeted drug delivery and environmental remediation of cytotoxic pharmaceuticals.

How to cite this article
Kadhim M., Kadam Z. Adsorption of Methotrexate onto Rosemary-Loaded Chitosan-Poly (Acrylic Acid)/MWCNTs Nanocomposite. J Nanostruct, 2025; 15(4):1607-1625. DOI: 10.22052/JNS.2025.04.011

INTRODUCTION

Drug delivery and nanomedicine have emerged as exciting fields of study in contemporary science, and they have drawn a lot of interest recently in both research and experimentation as well as several clinical trials [1-5]. The efficiency we need to transfer results from the lab to the patient's bedside will require cooperation between academic theory, laboratory experimentation, medical understanding, pharmaceuticals, and excellent research. Modern drug delivery technologies hold immense promise [6-9]. The targeted distribution of oral medication makes it an excellent therapy option for colon and stomach cancer. Hydrogels that are administered orally have also been demonstrated to improve solubility [10, 11], increase permeability across the gastrointestinal system, and modulate the activity of the glycoprotein B efflux pump, which is affected by drug resistance [12, 13]. Oral gels have shown significant mucous accessibility and durability with the gastrointestinal tract, in contrast to liposomes,

* *Corresponding Author Email: mohammed.kadhim.isa@atu.edu.iq*

micelles, and certain nanoparticles. The likelihood that chitosan, a monomer with a charged amino chain on the D-glucosamine residue, could react electrostatically with N-acetylnuraminic acid in the stomach mucous can account for the prolonged residence duration in the stomach [12].

Methotrexate is an immunosuppressive and anticancer drug that inhibits the metabolism of folic acid (vitamin B9) [13]. MTX prevents cell proliferation indirectly by inhibiting enzymes that bind folate, especially DHFR, which catalyzes the conversion of dihydrofolate to tetrahydrofolate (THF). DNA synthesis, repair, or replication depends on THF, a key cofactor in a number of methyltransferase activities in the pyrimidine and purine nucleotide production pathways [14, 15]. As medications, medicinal plants have been crucial in the treatment of various illnesses [16]. Because of their ability to heal a variety of illnesses, medicinal plants are increasingly being used in traditional medicine [17]. The advantage of herbal therapy is that, unlike synthetic medications, which have been shown to have serious side effects despite their potential to heal conditions, plants only contain natural ingredients. Numerous herbs have been shown to be effective in lowering blood sugar and high blood cholesterol, boosting the immune system, and offering some cancer prevention [18].

Rosemary is a perennial plant in the Lamiaceae family that is often used as a spice, especially in Mediterranean cooking. Carnosol, carnosic acid, and rosmarinic acid are in the rosemary extract, and α-pinene, bornyl acetate, camphor, and eucalyptol are in the essential oil [19]. It has been shown that carnosic acid and carnosol can affect the membranes of microbial cells by breaking up the lipid bilayer. This break makes the membrane more permeable, which lets ions, nucleotides, and proteins leak out of cells and causes cell lysis. Also, these chemicals have been shown to lower the amount of biofilm biomass by changing the expression of important genes that are involved in making biofilm [20]. People used it mostly in folk medicine because it could help with inflammation and fight bacteria [21]. Rosemary is one of the plants that has the most antioxidants [22]. Georgantelis et al. [23] reported that Hashemzadeh-Cigari et al. [24] found that a number of phenolic diterpenes, including carnosic acid, carnosol, rosmarinic acid, rosmanol, and rosmaridiphenol, are associated with the antioxidant properties of rosemary extract. The high antioxidant activity of the extract is a result of these compounds' ability to inhibit free radical chain reactions through metal ion chelation and electron donation. The most prevalent molecule in rosemary leaves and a crucial phenolic component, carnosic acid, has potent antioxidant qualities that surpass those of some artificial antioxidants [25]. As an uncommon food component that can be used in meals, rosemary extract is currently legally recognized under European legislation and assigned the E code E 392 [16, 17]. In comparison to black pepper, ginger, turmeric, and oregano, previous study has shown that using rosemary granules directly as a dry herb is the best strategy to prevent rapeseed oil from oxidizing [26]. In this study, we created a MWCNTs/hydrogel composite, added rosemary as a stabilizer to boost adoption efficiency, and then used the resultant composite of (CS-co-pAA-ROS) and MWCNTs to adopt the medication MTX.

The novelty of this study lies in the development of a rosemary-loaded chitosan-poly(acrylic acid)/MWCNTs nanocomposite for the adsorption of methotrexate (MTX), which has not been previously reported. Unlike earlier systems that utilized chitosan hydrogels or MWCNTs individually or in combination, our work uniquely incorporates rosemary powder, rich in phenolic diterpenes (carnosic acid, carnosol, rosmarinic acid), as a natural additive to enhance adsorption and drug release. Rosemary contributes antioxidant properties that facilitate hydrogen bonding and π–π interactions with MTX, improves the surface roughness and porosity of the composite (as shown by SEM and TEM), and enhances drug release efficiency up to 89%. Additionally, rosemary introduces potential biological synergies due to its known anti-inflammatory and anticancer effects. These features collectively make the composite a novel and multifunctional platform for MTX removal and controlled delivery.

MATERIALS AND METHODS

Materials

The rosemary came from one of Iraq's herbal factories. VCN Materials, Co., Ltd. in Iran gave the multiwall CNTs powder (pure 99%, OD = 40-60 nm, length = 5-10 um, surface area = 200 m^2/g, number of sheets = 7, thickness = 2.1 g/cm^3). HIMEDIA provided the medium molecular weight chitosan (96%). In Iraq, in India, a hospital administered methotrexate. We purchased acrylic

acid from Merck in Germany. We acquired acetic acid (99.5%) and MBA (99%) as cross-linkers from CDH in India. CDH, India, provided the initiator, potassium per sulfate (KPS), at 99%. N_2 gas. Fluka, Germany, supplied the HCl, KCl, NaOH, $CaCl_2$, and NaCl. Each solution was diluted with deionized water.

Preparation of (CS-co-pAA-ROSY/ MWCNTs) nanocomposite

The selection of rosemary, chitosan, and MWCNTs concentrations in the synthesis of the nanocomposite was based on a combination of preliminary experimental screening, literature guidance, and desired structural-functional outcomes. A chitosan concentration of 2.5% was chosen for its optimal viscosity and ability to form a stable hydrogel matrix, ensuring effective dispersion of both acrylic acid and MWCNTs. The MWCNTs were added at a concentration of 0.1% to provide structural reinforcement, enhance surface area, and improve mechanical strength without leading to aggregation, which becomes more likely at higher concentrations. Rosemary powder was incorporated at 0.1 g per 20 mL based on trials that showed this amount yielded significant enhancement in antioxidant content and surface functionality, while maintaining homogeneity and preventing phase separation. These specific ratios were found to balance dispersion stability, nanocomposite porosity, and drug loading efficiency, resulting in a synergistic structure with high adsorption performance toward MTX. Figure 1 show the graphical for preparation processing, 0.5 g of chitosan (CS) and 20 mL of 1% acetic acid were mixed to make a 2.5 weight percent chitosan solution. To finish the chitosan polymer dispersion, the resulting solution was agitated for 15 minutes at 60 ^{0}C. A 0.1% MWCNT solution was treated with an ultrasonic field for 10 minutes before being exposed to the CS solution. We finished the grafting method by swirling the CS/MWCNTs mixture at 70 ^{0}C. At this moment, CS macromolecules were adsorbed onto the surface of the MWCNTs, acting as a polymer cationic surfactant and stabilizing them [27]. The previous solution was used as a monomer by adding ten milliliters of acrylic acid (AA). Following the addition of KSP (0.02 g in 2 mL DI.W.) and the cross-linker MBA (0.02 g in 2 mL DI.W.), while stirring and bubbling the solution with nitrogen for 15 minutes to eliminate oxygen, After that, the mixture is mixed with the rosemary plant (ROSY) by dissolving 0.1 g of its powder in 20 mL of D.W. and letting it sit on a magnetic stirrer for half an hour. Afterward, we dissolve it in an ultrasonic apparatus. The plant is next added in the form of drips, and the combination is finally transferred to the water bath. The resultant nanocomposite was cut into equal pieces (5 mm) and rinsed many times with deionized water, changing the water every hour for 24 hours, to eliminate any unreacted monomers. After washing, the nanocomposite was dried to a consistent weight at 60 ^{0}C. The (CS-co-pAA-ROSY/MWCNTs) were

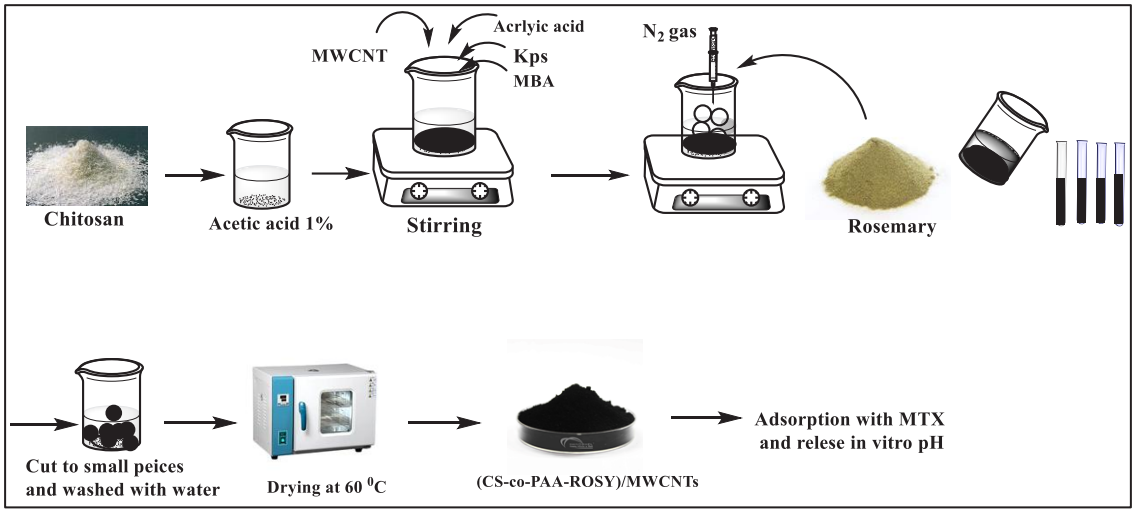

Fig. 1. Graphical synthetic route of (CS-co-PAA-ROSY/MWCNTs).

crushed, sieved, and kept in airtight containers for later usage [28]. Deionized water is the solvent used in the preparation process (Fig. 1).

The incorporation of rosemary in powder form for material synthesis was carefully optimized to ensure reproducibility and homogeneity. To achieve consistent results, the rosemary powder was sourced from a certified local herbal supplier, and each batch was visually inspected and weighed precisely. Prior to incorporation, the powder was dispersed in deionized water, sonicated, and magnetically stirred to promote uniform dissolution of bioactive compounds. Although a full phytochemical profiling (e.g., via HPLC or GC-MS) was not performed, literature data confirm that dried rosemary powder retains a stable composition of its key antioxidant constituents, including carnosic acid, rosmarinic acid, and carnosol. Moreover, the reproducibility was ensured by maintaining constant processing conditions (temperature, time, mixing rate) and using identical preparation protocols for each batch. Future studies will consider conducting quantitative analyses of rosemary's active constituents to better control batch-to-batch variation and confirm bioactivity levels more precisely.

Characterization

Fourier transform infrared (FTIR) spectra of the nanocomposite were recorded using a Bruker (Germany) Equinox 55, Tensor 27, KBr, at a wavelength of 400–4000 cm^{-1}. X-ray diffraction (XRD) was obtained using a Philips (USA) diffractometer (Model: PW1730). The products were examined microscopically using a Philips (Netherlands) electron microscope (Model: EM208S) and a Tescan (Czech Republic) FESEM. A Zetaser Nano-ZS from Malvern Instrument was used for zeta potential determination. The EDX instrument is similar to the FESEM except for detector (SE) modifications.

Adsorption Isotherm

Batch adsorption studies are performed to gather preliminary data to establish the best parameters for drug removal effectiveness, such as concentration, equilibrium time, temperature, ionic strength, and pH. Several sets of these steps are executed: 10 ml of the 25 $mg.L^{-1}$ MTX solution and 0.05 g of the nanocomposite are placed in separate conical flasks. The mixtures are shaken at 140 rpm until equilibrium is reached, then centrifuged at 4000 rpm for 10 minutes. The equation calculates the drug's adsorption capacity, and calibration curves are used to get the equilibrium concentration (Eq. 1) [29]:

$$\text{Qe or } \frac{x}{m} = \frac{V(Co - Ce)}{m} \quad (1)$$

The efficiency of drug adsorption (E%) is determined using the equation below [30]:

$$E\% = \frac{(Co - Ce)}{Co} \times 100 \quad (2)$$

Where: C_o ($mg.L^{-1}$) and C_e ($mg.L^{-1}$) stand for the starting and equilibrium drug concentrations, respectively, and x is the amount of drug adsorbed, whereas m (g) is the mass of the adsorbent material. Qe ($mg.g^{-1}$) is the amount of drug adsorbed at equilibrium [31-33].

To evaluate the reusability and regeneration performance of the synthesized CS-co-pAA-ROSY/MWCNTs nanocomposite, five consecutive adsorption–desorption cycles were carried out under batch conditions. Initially, methotrexate (MTX) was adsorbed from an aqueous solution (25 mg/L, pH 4) over a contact time of 90 minutes. The spent adsorbent was then separated, rinsed with deionized water, and subjected to desorption using three different media: 0.1 M NaOH (basic), distilled water (neutral), and 0.1 M HCl (acidic). In each desorption step, 10 mL of the respective solution was added to the MTX-loaded nanocomposite and stirred at room temperature for 30 minutes. After desorption, the adsorbent was washed, recovered, and reused in the subsequent adsorption cycle under the same conditions. The removal efficiency (%) for each cycle was determined using UV-Vis spectroscopy at 303 nm.

RESULTS AND DISCUSSION

Characterization of (CS-co-pAA-ROSY/ MWCNTs) nanocomposite

Fig. 2 depicts the FTIR spectra of the nanocomposite (CS-co-PAA-ROSY/MWCNTs) before (black) and after (red) loading methotrexate (MTX). Spectrum (a) shows characteristic peaks of chitosan, poly (acrylic acid), and rosemary components as O–H and N–H stretching near 3400

cm^{-1}, carbonyl (C=O) stretching around 1716 cm^{-1}, and C–O vibrations. As demonstrated in spectrum (b), significant changes were noted, including peak shifts and intensity reductions in the carbonyl and amine regions, which are consistent with hydrogen bonding or ionic interactions. These alterations show that MTX was successfully loaded onto the nanocomposite via hydrogen bonding or ionic interactions with functional groups in the hydrogel matrix. As shown in Fig. 3, the (CS-co-PAA-ROSY/MWCNTs) nanocomposite's XRD pattern before (black) and after (red) loading methotrexate (MTX). The broad peak at 20.07° confirmed the amorphous nature of the polymeric matrix.

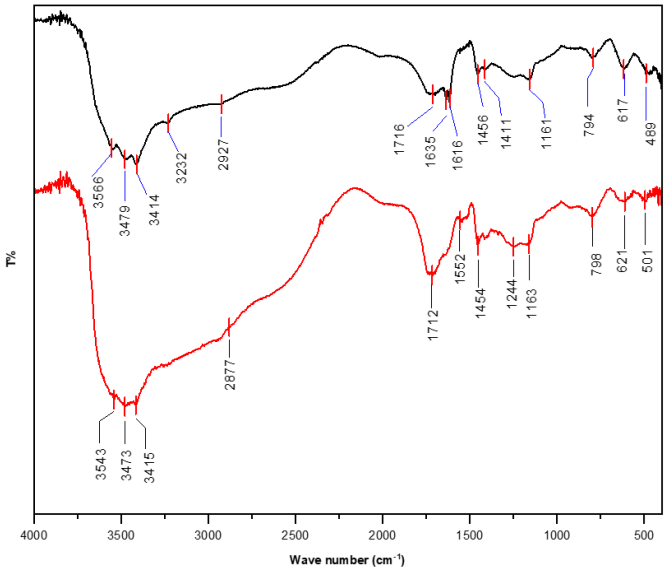

Fig. 2. FTIR of nanocomposite (CS-co-PAA-ROSY/MWCNTs) (black) before (red) after loaded MTX.

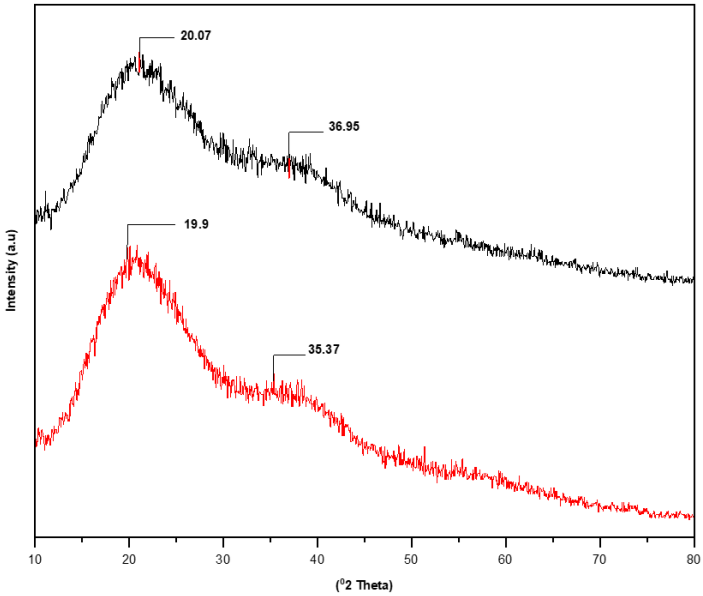

Fig. 3. XRD of nanocomposite (CS-co-PAA-ROSY/MWCNTs) (black) before (red) after loaded MTX.

Polyacrylic acid is responsible for the considerable diffraction at 36.95°. After MTX loading, the primary peak moved slightly to 19.9°, and a new band emerged at 35.37°, demonstrating that the drug may be dispersed within the polymeric matrix without causing crystallinity to occur [34-39].

Fig. 4 (a-d) depicts SEM images of the (CS-co-PAA-ROSY/MWCNTs) composite before and after methotrexate loading. The surface of the composite has a rough, non-smooth texture, which enhances its specific surface area. Additionally, porosity is visible on the surface of the (CS-co-pAA-ROSY/MWCNTs), resulting in better adsorption properties. TEM micrographs of the (CS-co-pAA-ROSY/MWCNTs) composite are shown in Fig. 5(a-d) both before and after MTX loading. There are no discernible MWCNTs in the TEM images, suggesting high homogeneity and a significant impact of chitosan on carbon nanotubes. The composite's highly porous architecture and high specific surface area are a result of the micrographs' depiction of a porous, hollow structure with irregularly shaped particles and apparent lines of aligned pores [39-41].

SEM and TEM images show that the composite is amorphous and give information about its

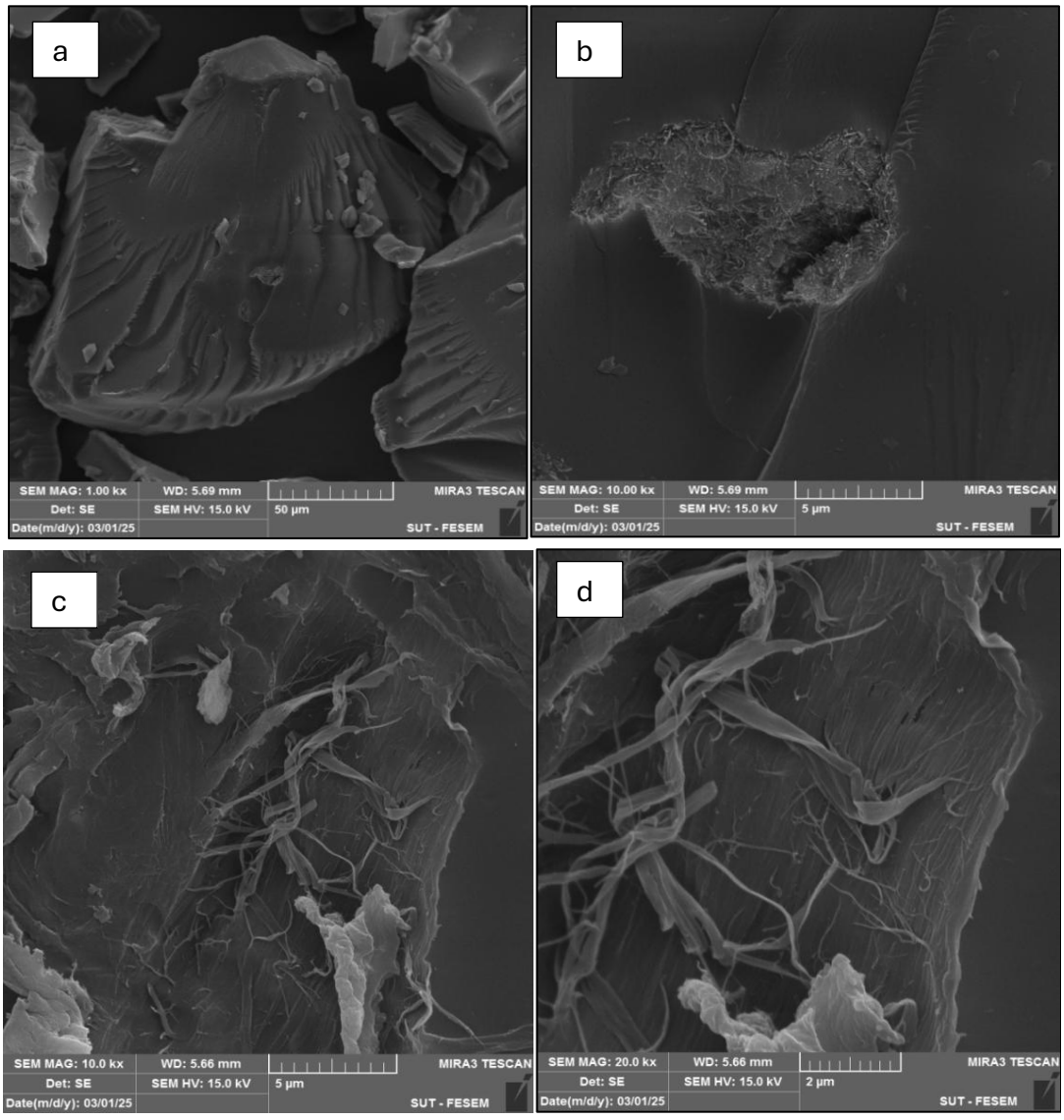

Fig. 4. FESEM Micrographs of (CS-co-PAA-ROSY/MWCNTs), (a,b)before (c,d)after loaded MTX.

structure. Fig. 6 (a,b) shows the EDS (Energy Dispersive Spectroscopy) analysis, which shows the percentage values of the elements in the composite. Fig. 6 (b,d) shows the same thing [42, 43].

The (CS-co-PAA-ROSY/MWCNTs) nanocomposite was found to have a significant anionic charge (Fig. 7). The zeta potential of the (CS-co-pAA-ROSY/MWCNTs) nanocomposite was measured to be –46.5 mV, indicating a strongly negative surface charge. This high negative zeta potential enhances electrostatic attraction between the nanocomposite and the positively charged or protonated functional groups of methotrexates (MTX), especially at acidic pH where MTX remains largely in its protonated form. The negative surface potential also contributes to colloidal stability, preventing aggregation of nanocomposite particles and ensuring uniform dispersion during adsorption. As a result, the strong negative zeta potential is directly related to the high adsorption efficiency observed in the system, particularly at pH 4. Thus, zeta potential is a critical parameter in understanding the electrostatic interactions driving MTX adsorption onto the composite surface [38].

Adsorption study

Calibration Curve of Methotrexate (MTX) drug

The MTX medication was diluted in a number of processes to produce solutions containing varying quantities of the drug. We assessed the absorbance of MTX solutions at 303 nm (λ max) using the sophisticated Shimadzu PC 1800 ultraviolet-visible spectrophotometer. Fig. 8 depicts a strong plot of these absorption values against

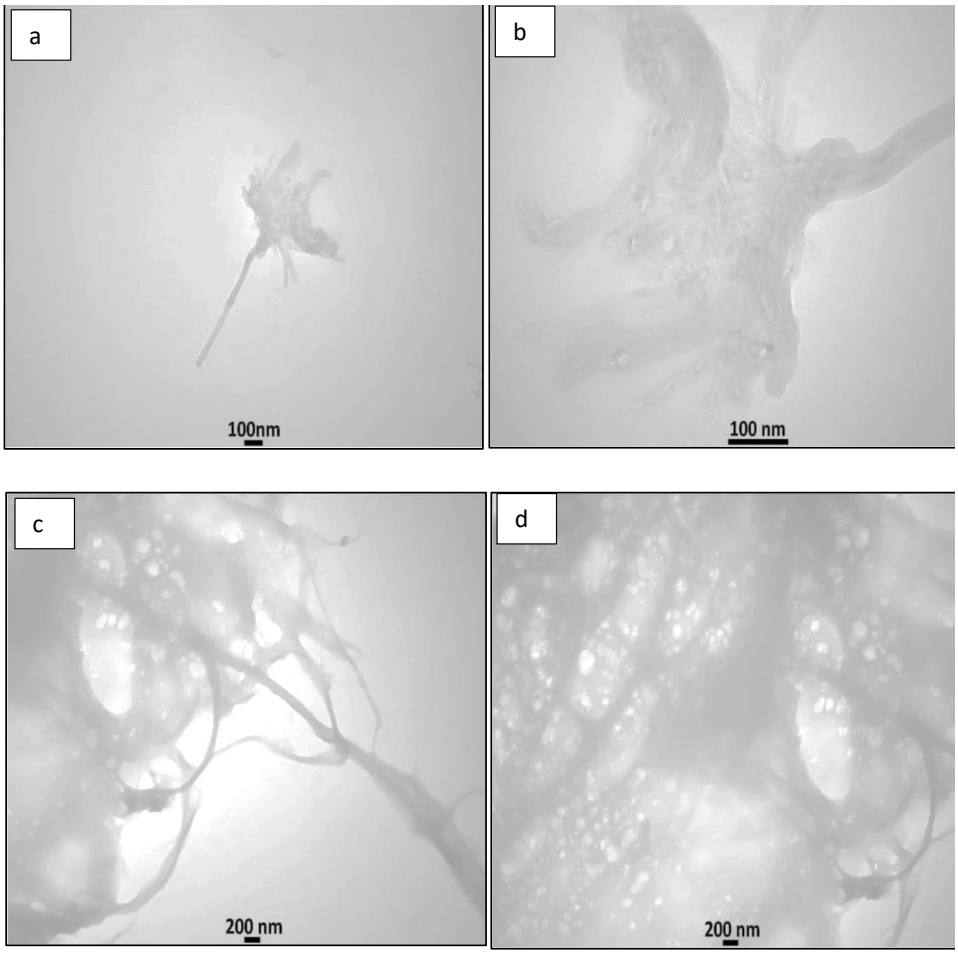

Fig. 5. TEM Micrographs of (CS-co-PAA-ROSY/MWCNTs), (a,b)before (c,d)after loaded MTX.

the MTX concentrations associated with them. This graphic not only illustrates the relationship between concentration and absorption, but it also demonstrates that Beer-Lambert's law applies in this concentration range. As a consequence, it is feasible to create a powerful MTX calibration

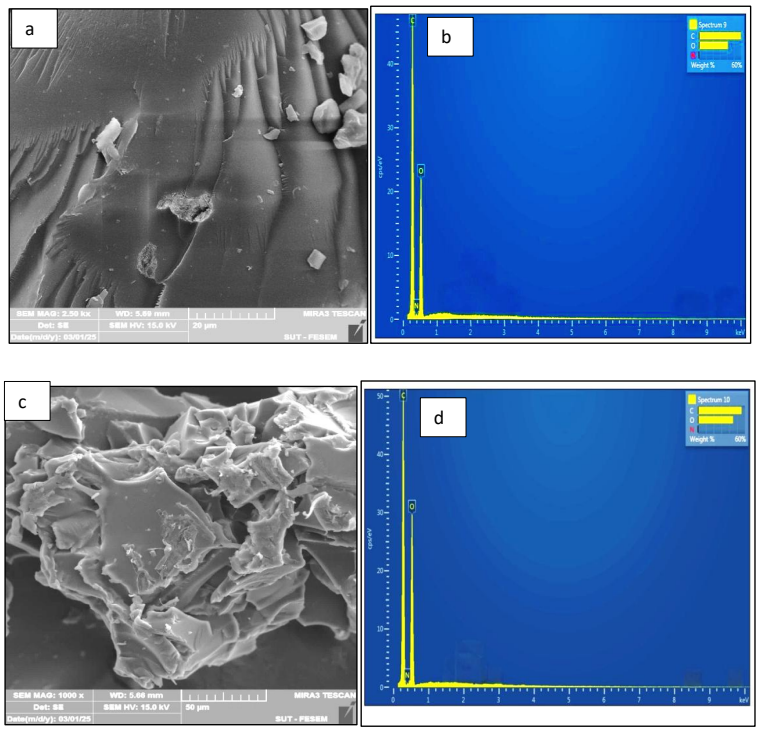

Fig. 6. EDS and EDX Micrographs of (CS-co-PAA-ROSY/MWCNTs), (a, b) before (C, d) after loaded MTX .

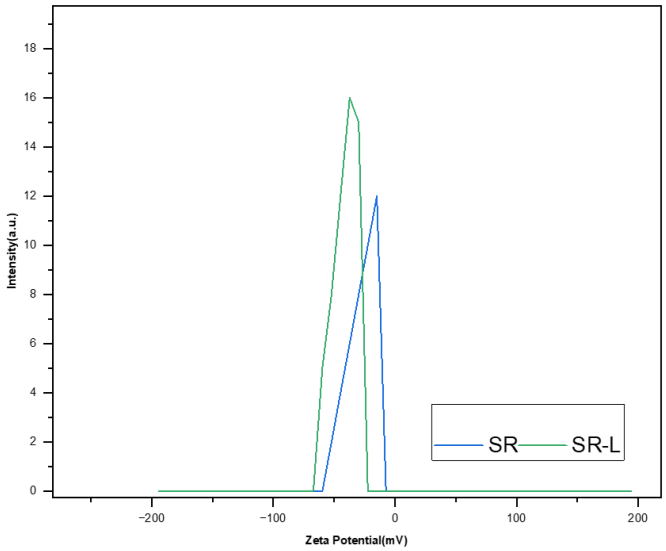

Fig. 7. Zeta potential distribution for the (CS-co-PAA-ROSY/MWCNTs), (SR) before (SR-L) after loaded MTX.

curve.

The impact of interaction time

Fig. 9 shows how contact time affects medicine absorption by the (CS-co-pAA-ROSY/MWCNTs) nanocomposite. Throughout the first 10 minutes, the amount of drug adsorbed rapidly rises, suggesting that all active sites of the adsorbent material are being used. Following the initial time, the adsorption rate progressively increases until it hits a plateau. The optimal adsorption time for the medicine with the (CS-co-pAA-ROSY/MWCNTs) nanocomposite was determined to be 90 minutes, since only a tiny change in the amount of drug adsorbed was seen after this time [44-47].

Effect of temperature

Using drug concentrations ranging from 10 to 100 mg. L^{-1}, the effect of temperature on adsorption was examined for 90 minutes at 15 to 30°C. The adsorption process is exothermic, as shown by the results in Fig. 10. In particular, when the temperature dropped, more MTX medication was absorbed. This result suggests that molecules may have more kinetic energy at lower temperatures, which would lessen their likelihood of interacting with the adsorbent [48-50]. The amount of MTX adsorbed was found

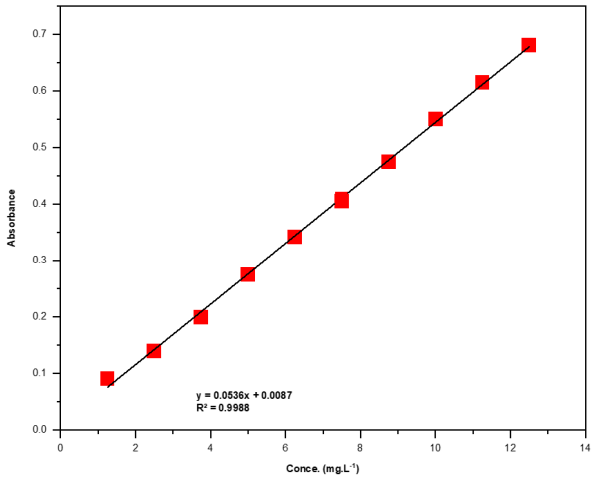

Fig. 8. Calibration curve of the MTX drug.

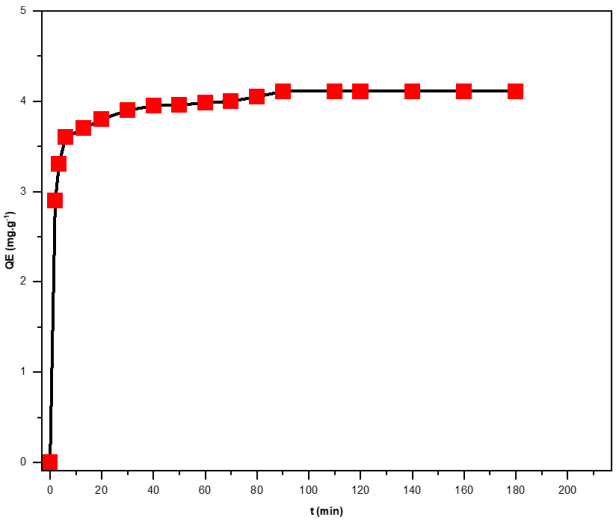

Fig. 9. The effect of contact time on MTX adsorption.

to be reasonable when compared to ambient temperatures, with no discernible decrease in adsorption from 15 to 30 °C.

Effect of pH

In testing solutions containing 0.1 mol. L^{-1} HCl and 0.1 mol. L^{-1} NaOH in pH ranges of 2 to 12, the (CS-co-pAA-ROS)/MWCNTs nanocomposite efficiently eliminates methotrexate (MTX). The results of these findings are displayed in Fig. 11. While MTX clearance peaked at pH 4, elimination efficiency rose from pH 2 to pH 7. Because the adsorbate ionizes and acquires a negative charge, this removal is most effective at this pH [51]. Polyacrylic acid and chitosan's positive charges combine to produce electrostatic interactions with the drug. Polyacrylic acid contains carboxyl groups (COOH), while chitosan contains amino groups (NH_2). NH_3^+ and $COOH_2^+$ are released into the aqueous solution when positively charged. Moreover, the drug becomes protonated when the pH rises above the pKa values (methotrexate (MTX) has a pKa of 4.05, for instance). Drug adsorption is reduced at higher pH values because of the repulsive force exerted by the adsorbents' positive charges [52]. The proposed adsorption mechanism of methotrexate (MTX) onto the (CS-co-pAA-ROSY/MWCNTs) nanocomposite is

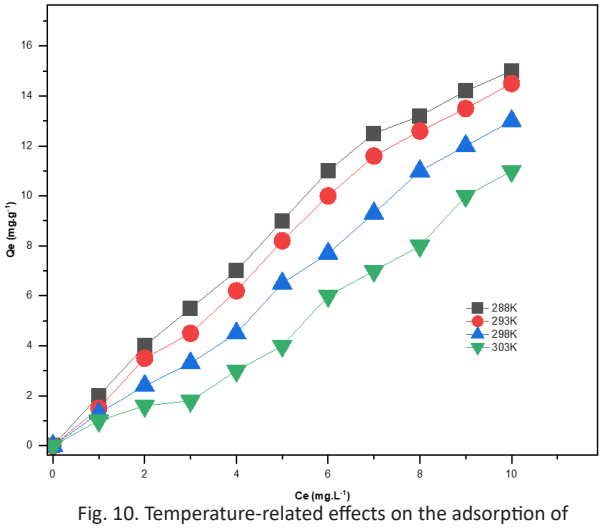

Fig. 10. Temperature-related effects on the adsorption of

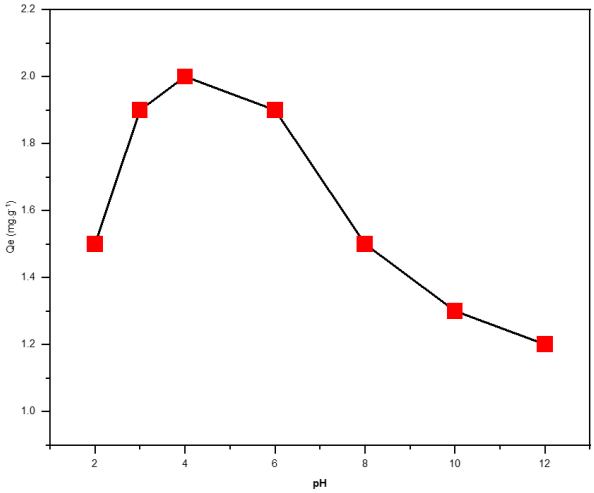

Fig. 11. Effect of pH in the MTX adsorption.

primarily based on hydrogen bonding and ionic interactions between the functional groups of MTX and the hydroxyl, amino, and carboxyl groups present on the composite surface. This is supported by changes observed in FTIR spectra (shifted or diminished peaks), zeta potential measurements (–46.5 mV indicating strong surface charge), and pH-dependent adsorption behavior.

Ionic strength's effect

The effect of competing ions was studied by introducing various salts (NaCl, KCl, $CaCl_2$) into the MTX solution at different concentrations to evaluate their influence on adsorption efficiency. The results, presented in Fig. 12, show a noticeable decrease in MTX adsorption with increasing salt concentration, due to competition between MTX and cations for available adsorption sites on the nanocomposite surface. Additionally, ionic shielding effects reduce electrostatic interactions, especially under higher ionic strength. Notably, calcium ions had a less pronounced inhibitory effect compared to sodium and potassium ions, likely due to their lower mobility and larger hydration radius. These findings suggest that while ionic strength does influence adsorption performance, the (CS-co-pAA-ROSY/MWCNTs) nanocomposite retains reasonable selectivity toward MTX even in the presence of competing ions, making it suitable for use in complex aqueous environments [53].

Adsorption Isotherm Models

The adsorption isotherm describes the connection between the concentration of adsorbate in the solution and the temperature-dependent amount of material adsorbed. The adsorption equilibrium data is analyzed using the Langmuir, Temkin, and Freundlich isotherms. Typically, a linear relationship is discovered, and the suitability of the isotherm equations is evaluated using correlation coefficients. A direct relationship between log Ce and log Qe is shown by the Freundlich isotherm. This correlation suggests that the ions of the MTX medication follow the Freundlich isotherm, as shown by the correlation coefficient shown in Fig. 13a-c and Table 1. Among these, the Freundlich model exhibited the best fit with the experimental data, indicated by a high correlation coefficient (R^2 = 0.9942), compared to Langmuir (R^2 = 0.6433) and Temkin (R^2 = 0.9261). This suggests that the adsorption of MTX onto the (CS-co-pAA-ROSY/MWCNTs) nanocomposite occurs on a heterogeneous multilayer surface with different energy binding sites, as described by the Freundlich model. The model also reflects favorable adsorption conditions with a Freundlich constant (K_F) of 9.903 and an exponent (n) value near 1.0. These results confirm the material's

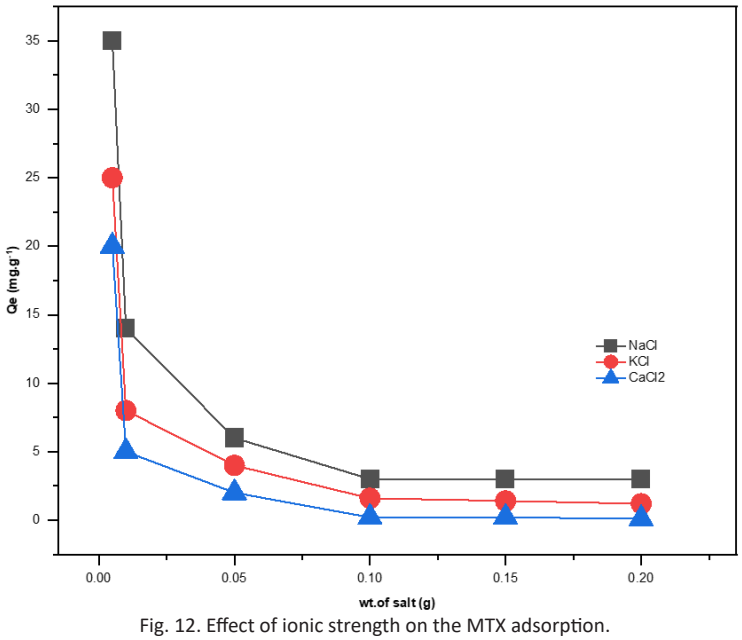

Fig. 12. Effect of ionic strength on the MTX adsorption.

suitability for practical adsorption applications and support the proposed adsorption mechanism involving multiple interactions [53].

Adsorption thermodynamics

Calculating values of Xm at various solution temperatures allowed for the estimation of

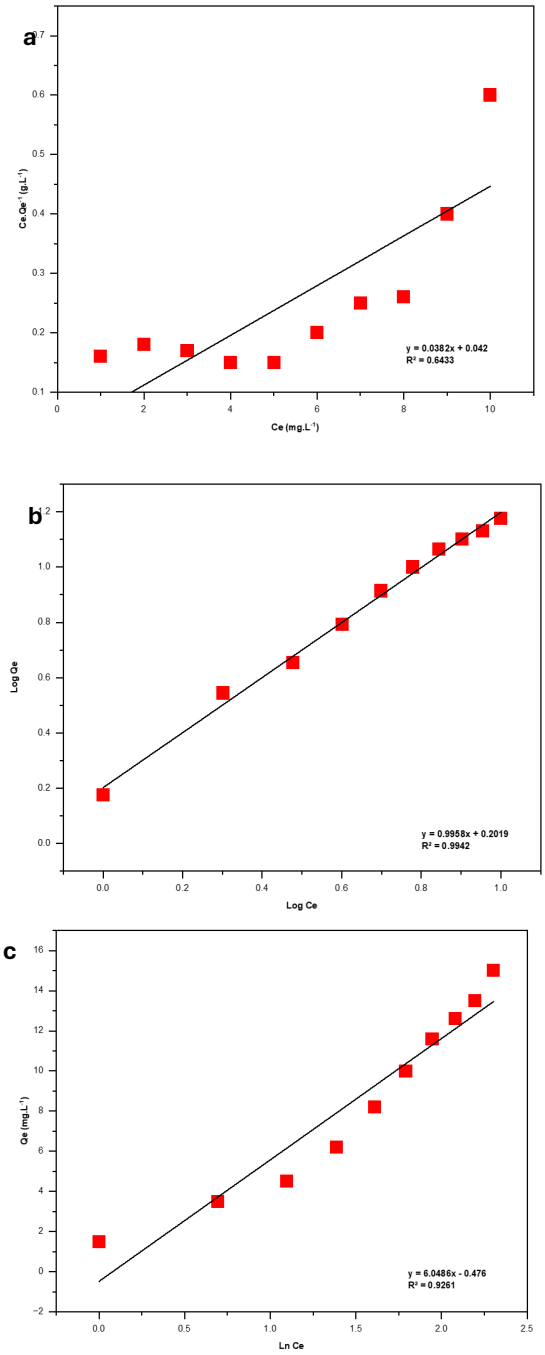

Fig. 13. Adsorption isotherms of: a- Langmuir, b-Freundlich and c-Timken equations.

the fundamental thermodynamic quantities of MTX drug adsorption on the (CS-co-pAA-ROS)/ MWCNTs nanocomposite. In Fig. 14, The enthalpy (ΔH), entropy (ΔS), and free change energy (ΔG) are calculated using Eq 3-5:

$$\Delta G = \Delta H\text{-}T.\Delta S \quad (3)$$

$$\Delta G = -RT \ln K_{eq} \quad (4)$$

$$\ln Keq = -\frac{\Delta H}{RT} + \frac{\Delta S}{R} \quad (5)$$

The temperature value of the surface absorption of the MTX drug is shown in Table 2. The negative Free Gibbs energy (ΔG) of the nanocomposite (CS-co-pAA-ROSY/MWCNTs) causes spontaneous adsorption [54]. Because the enthalpy value is less than 40 kJ/mol and the adsorption process is exothermic, methotrexate primarily adsorbs onto the nanocomposite surface by physical means. The particles adsorbed on the surface of the polymer adsorbent are less mobile and more organized, as indicated by the negative decrease in entropy (ΔS).

Adsorption kinetics

Kinetic process analysis requires knowledge of the dynamic reaction and investigation of the adsorption conditions. A range of kinetic models have been used to assess experimental data in order to determine the adsorption process and control phase. Several models, such as intraparticle diffusion, pseudo-first-order, and pseudo-second-order kinetic models, were used to determine the kinetic equation for the adsorption process. Eq. 6 represents this pseudo-first-order kinetic model

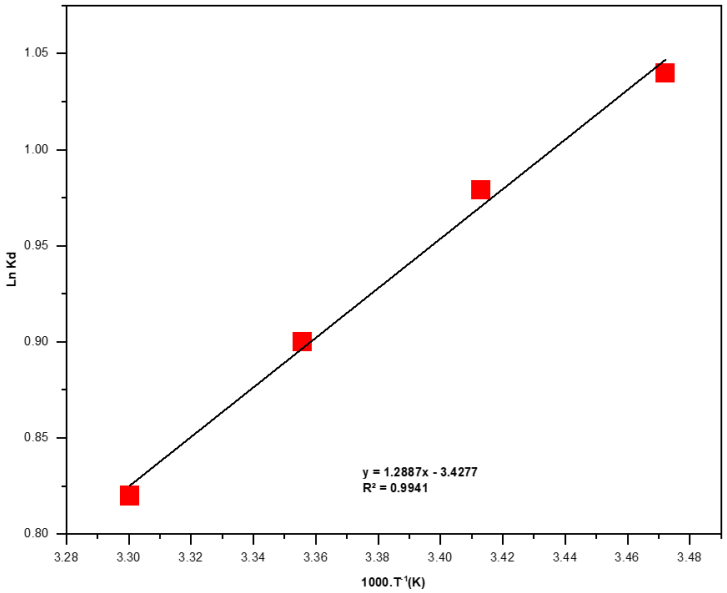

Fig. 14. showing the relationship between Ln Kd and reciprocal absolute temperature for MTX medication adsorption.

Table 1. The Langmuir, Freundlich and Timken, correlation coefficients and constants of MTX adsorption.

Langmuir equation			Freundlich equation			Timken equation		
K_L	q_{max}	R^2	K_F	N	R^2	K_T	B	R^2
1.099476	26.17801	0.6433	9.903	1.0042	0.9942	0.924	6.0486	0.9261

[55].

$$Ln(q_e - q_t) = \ln(q_e) - k_l \cdot t \quad (6)$$

The ln(qe - qt) linear plot is shown as a function of time (t). Table 3 and Fig. 15 contain pertinent data about MTX. The rate at which the adsorbent's active participants are filled is directly proportional to the quantity of vacant spaces, as per the pseudo-first-order kinetic model. According to the pseudo-second-order model, the sharing or exchange of electrons between the adsorbent and adsorbate controls the rate of surface adsorption. The following formula represents the pseudo-second-order model model [55].

$$\frac{1}{q} = \frac{1}{kh.\,qe2} + \frac{t}{qe} \quad (7)$$

The constant k_h is defined as a pseudo-second-order rate constant ($g.mg^{-1}\ min^{-1}$).

The values of q_e and k_h obtained by charting methotrexate (MTX) adsorption on the (CS-co-pAA-ROSY/MWCNTs) nanocomposite are displayed in Table 3 and Fig. 16. The intercept and slope of the lines at various concentrations were

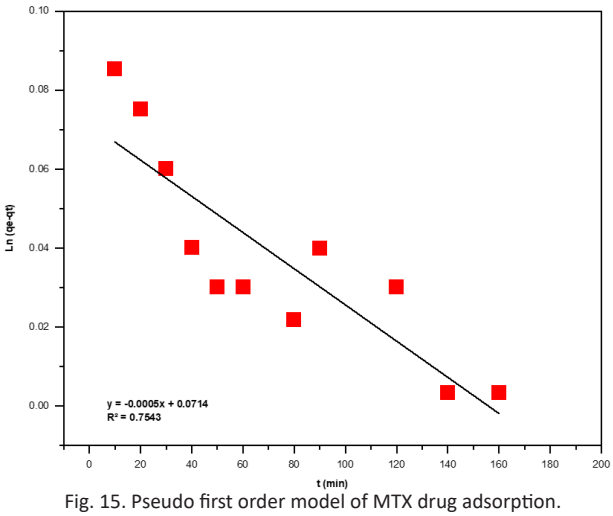

Fig. 15. Pseudo first order model of MTX drug adsorption.

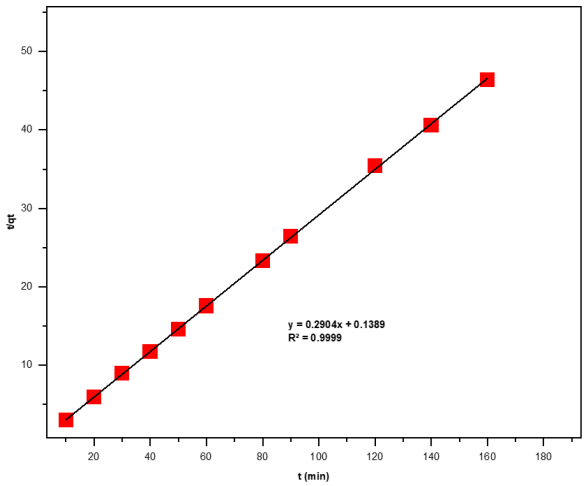

Fig. 16. Pseudo second order model of MTX drug adsorption.

used to estimate these values. The MTX adsorption process kinetics seem to be sufficiently explained by the pseudo-second-order equation for the (CS-co-pAA-ROSY/MWCNTs) nanocomposite. This is clear because the calculated adsorption capacity (q_{cal}) and the observed adsorption capacity (q_{exp}) are nearly the same. Therefore, this model offers a higher coefficient of correlation than earlier kinetics theories. higher correlation value compared to alternative kinetic models.

Drug Loading Efficiency and Release

Fig. 17 shows the drug release from the (CS-co-pAA-ROSY/MWCNTs) nanocomposite was examined in three different ways at various pH values. The maximum efficiency of 89% was attained by MTX loading. Plotted against time (hours), the graph displays the cumulative percentage of drug

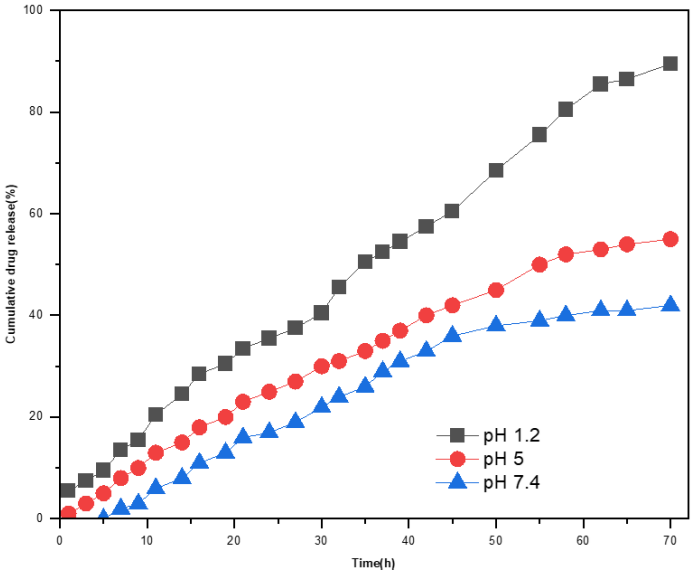

Fig. 17. In-vitro release of MTX from MTX-loaded (CS co-PAA-ROSY)/MWCNTs nanocomposites at different pH conditions.

Table 2. Shows the thermal value of the MTX drug's surface absorption.

(CS-co-pAA-ROSY/MWCNTs)			
T(K)	ΔG (kJ/mol)	ΔH (kJ/mol)	ΔS (J/mol.K)
288	-2.51261		
293	-2.37012		
298	-2.22763	-10.7143	-28.4979
303	-2.08514		

Table 3. Pseudo first and second order model of MTX drug adsorption.

Adsorbent	Pseudo-first order			Pseudo-second order			
	K_1	$q_{e\ (cal)}$	R^2	K_2	q_e(cal)	h	R^2
(CS-co-pAA-ROSY/MWCNTs)	0.0005	1.1	0.7543	0.607533	3.443526	7.201	0.9999

release, averaged over three replicates. Over the course of 72 hours, release tests were conducted at different pH values. The sample membrane expanded due to pharmacological diffusion, resulting in the first "burst" pharmacological effect. Due to the porosity of the nanocomposite, the drug was released to the surface of the sample much more quickly than it was deep inside [56]. The swelling process results are in line with the nanocomposite's higher MTX release at pH 1.2 compared to pH 5 and 7.4. Methotrexate dissolves the least in the pH range of neutral. Consequently, the release results demonstrate that, unlike the dissolving process, where a high swelling ratio leads to the enlargement of the nanocomposite's pores, the amount of swelling in the nanocomposite controls its release. It is evident that 89% of the methotrexate was liberated from the nanocomposite at 72 hours due to the diffusion of the drug through the larger pore size observed at pH = 1.2. The rate of drug release was 41% at pH = 7.4 and 55% at pH = 5. The significantly reduced swelling capacity of the nanocomposite is responsible for the significantly reduced drug release. By making the hydrogel surface rougher, the addition of rosemary increased drug adsorption and release efficiency compared to previous studies that used hydrogels without the plant rosemary [2].

Reusability Results

The results, as depicted in the Fig. 18 reveal significant differences in regeneration efficiency among the tested media. The acidic medium (0.1 M HCl) exhibited the highest retention of adsorption capacity over five cycles, with removal efficiency decreasing only slightly from 94.8% in the first cycle to 88.9% in the fifth. This suggests strong structural stability of the nanocomposite in acidic conditions and effective desorption of methotrexate (MTX), likely due to protonation of surface functional groups that facilitates drug release. In contrast, the neutral medium (distilled water) showed moderate performance, with efficiency declining from 64.7% to 30.3%, indicating incomplete desorption and potential surface fouling or loss of active sites. The basic medium (0.1 M NaOH) demonstrated the poorest regeneration, with a sharp drop from 36.2% to 6.7%, possibly due to the degradation or deactivation of functional groups such as amino and carboxyl groups under alkaline conditions or strong MTX binding caused by deprotonation. These findings confirm that regeneration in acidic media is the most effective approach, as the nanocomposite maintained over 88% of its adsorption capacity after five

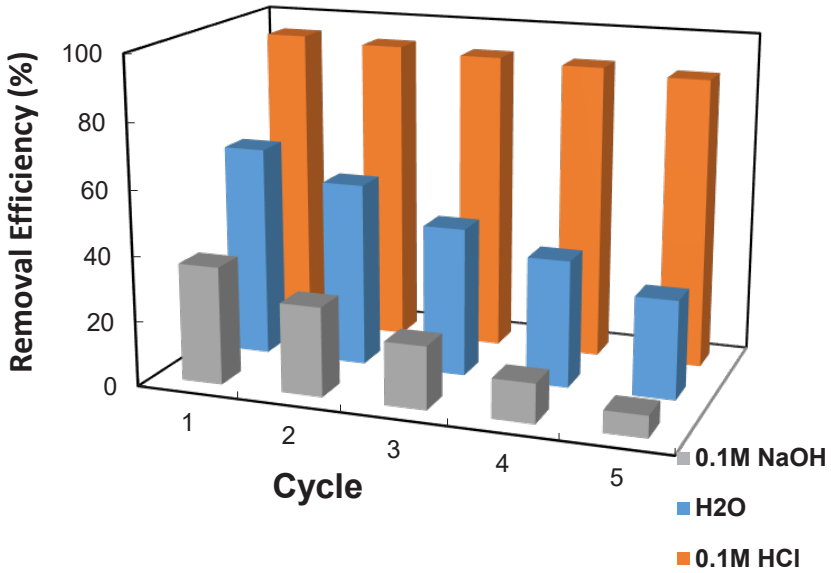

Fig. 18. Removal Efficiency of MTX by CS-co-pAA-ROSY/MWCNTs Nanocomposite Over Five Adsorption–Desorption Cycles Using Different Regeneration Media.

cycles, demonstrating excellent reusability and promising potential for drug removal in aqueous environments [57, 58].

CONCLUSION

The (CS-co-pAA-ROSY/MWCNTs) nanocomposites were successfully synthesized and efficiently used for the adsorption of MTX from aqueous solutions. The integration of rosemary (Rosmarinus officinalis) into the drug delivery system with methotrexate (MTX) is based on its well-documented antioxidant, anti-inflammatory, and potential anticancer properties [40,41]. Rosemary contains bioactive compounds such as carnosic acid, rosmarinic acid, and ursolic acid, which have been shown to induce apoptosis and inhibit proliferation in various cancer cell lines [42]. These compounds may synergize with MTX by enhancing its cytotoxic effects or modulating the tumor microenvironment. Additionally, the presence of rosemary may improve the bioavailability or controlled release profile of MTX when incorporated within the hydrogel matrix, potentially leading to more effective and targeted delivery. The Freundlich adsorption model indicates that the (CS-co-pAA-ROSY/MWCNTs) nanocomposite can readily and efficiently adsorb the MTX drug (K_F = 9.903 and n = 1.004218). Contact time = 90 min, starting adsorbate concentration = 25 mg. L^{-1}, pH = 4 at 293 K. Thermodynamic parameters with negative values ΔG = -2.37 kJ/ mol , ΔH= -10.72 kJ/ mol and ΔS = -28.5 J/mol.K indicate that this adsorption is exothermic.

CONFLICT OF INTEREST

The authors declare that there is no conflict of interest regarding the publication of this manuscript.

REFERENCES

1. Chow EK-H; Ho D. Cancer nanomedicine: from drug delivery to imaging. Science translational medicine. 2013;5(216):216rv214-216rv214.
2. Malik S; Muhammad K; Waheed Y. Emerging applications of nanotechnology in healthcare and medicine. Molecules. 2023;28(18):6624.
3. Yusuf A; Almotairy ARZ; Henidi H; Alshehri OY; Aldughaim MS. Nanoparticles as drug delivery systems: a review of the implication of nanoparticles' physicochemical properties on responses in biological systems. Polymers. 2023;15(7):1596.
4. Foulkes R; Man E; Thind J; Yeung S; Joy A; Hoskins C. The regulation of nanomaterials and nanomedicines for clinical application: current and future perspectives. Biomaterials science. 2020;8(17):4653-4664.
5. Ma X; Tian Y; Yang R; Wang H; Allahou LW; Chang J; Williams G; Knowles JC; Poma A. Nanotechnology in healthcare, and its safety and environmental risks. Journal of nanobiotechnology. 2024;22(1):715.
6. Singh A; Amiji MM. Application of nanotechnology in medical diagnosis and imaging. Current opinion in biotechnology. 2022;74:241-246.
7. Barbosa AI; Rebelo R; Reis RL; Bhattacharya M; Correlo VM. Current nanotechnology advances in diagnostic biosensors. Medical Devices & Sensors. 2021;4(1):e10156.
8. Sardari S; Hheidari A; Ghodousi M; Rahi A; Pishbin E. Nanotechnology in tissue engineering: expanding possibilities with nanoparticles. Nanotechnology. 2024;35(39):392002.
9. Mura S; Nicolas J; Couvreur P. Stimuli-responsive nanocarriers for drug delivery. Nature materials. 2013;12(11):991-1003.
10. Allen TM; Cullis PR. Liposomal drug delivery systems: from concept to clinical applications. Advanced drug delivery reviews. 2013;65(1):36-48.
11. Elsabahy M; Wooley KL. Design of polymeric nanoparticles for biomedical delivery applications. Chemical Society Reviews. 2012;41(7):2545-2561.
12. Maeda H. Tumor-selective delivery of macromolecular drugs via the EPR effect: background and future prospects. Bioconjugate chemistry. 2010;21(5):797-802.
13. Prabhu P; Patravale V. The upcoming field of theranostic nanomedicine: an overview. Journal of Biomedical Nanotechnology. 2012;8(6):859-882.
14. Lim C; Lee S; Han D; Lee C; Kim BJ. Composition-Tolerant Terpolymers for Efficient, Nonhalogenated Solvent-Processed Polymer Solar Cells. Macromolecules. 2022;55(23):10395-10404.
15. Gupta P; Garcia E; Sarkar A; Kapoor S; Rafiq K; Chand HS; Jayant RD. Nanoparticle based treatment for cardiovascular diseases. Cardiovascular & Haematological Disorders-Drug Targets (Formerly Current Drug Targets-Cardiovascular & Hematological Disorders). 2019;19(1):33-44.
16. Silaghi A; Constantin VD; Socea B; Banu P; Sandu V. Journal of Mind and Medical Science s. Sciences.10(2):4.
17. Keshamma E; Patra KK; Pandey A; Kumar A; Singh N; Ghoshal S; Ghosh T; Pathak V; Raikwar CK. International Journal of Modern Pharmaceutical Research.
18. Ribeiro-Santos R; Carvalho-Costa D; Cavaleiro C; Costa HS; Albuquerque TG; Castilho MC; Ramos F; Melo NR; Sanches-Silva A. A novel insight on an ancient aromatic plant: The rosemary (Rosmarinus officinalis L.). Trends in Food Science & Technology. 2015;45(2):355-368.
19. Nieto G; Ros G; Castillo J. Antioxidant and antimicrobial properties of rosemary (Rosmarinus officinalis, L.): A review. Medicines. 2018;5(3):98.
20. Arranz E; Mes J; Wichers HJ; Jaime L; Mendiola J; Reglero G; Santoyo S. Anti-inflammatory activity of the basolateral fraction of Caco-2 cells exposed to a rosemary supercritical extract. Journal of Functional Foods. 2015;13:384-390.
21. Peng Y; Yuan J; Liu F; Ye J. Determination of active components in rosemary by capillary electrophoresis with electrochemical detection. Journal of pharmaceutical and biomedical analysis. 2005;39(3-4):431-437.
22. Georgantelis D; Blekas G; Katikou P; Ambrosiadis I; Fletouris DJ. Effect of rosemary extract, chitosan and α-tocopherol on lipid oxidation and colour stability during frozen storage of beef burgers. Meat science. 2007;75(2):256-264.

23. Hashemzadeh-Cigari F; Khorvash M; Ghorbani G; Kadivar M; Riasi A; Zebeli Q. Effects of supplementation with a phytobiotics-rich herbal mixture on performance, udder health, and metabolic status of Holstein cows with various levels of milk somatic cell counts. Journal of Dairy Science. 2014;97(12):7487-7497.
24. Gutiérrez CLM; Medina DIT; Jaramillo-Flores ME. Peppers and spice capsicum. Handbook of vegetable preservation and processing. 2015:580-609.
25. Veras KS; Fachel FNS; Pittol V; Garcia KR; Bassani VL; Dos Santos V; Henriques AT; Teixeira HF; Koester LS. Compatibility study of rosmarinic acid with excipients used in pharmaceutical solid dosage forms using thermal and non-thermal techniques. Saudi Pharmaceutical Journal. 2019;27(8):1138-1145.
26. Meng J; Wang Z-G; Zhao X; Wang Y; Chen D-Y; Liu D-L; Ji C-C; Wang T-F; Zhang L-M; Bai H-X. Silica nanoparticle design for colorectal cancer treatment: Recent progress and clinical potential. World Journal of Clinical Oncology. 2024;15(6):667.
27. Mandal TK; Bostanian LA; Graves RA; Chapman SR; Womack I. Development of biodegradable microcapsules as carrier for oral controlled delivery of amifostine. Drug Dev Ind Pharm. 2002;28(3):339-344.10.1081/ddc-120002849.
28. Urooj H; Javed T; Taj MB; Nouman Haider M. Adsorption of crystal violet dye from wastewater on Phyllanthus emblica fruit (PEF) powder: kinetic and thermodynamic. International Journal of Environmental Analytical Chemistry. 2024;104(19):7474-7499.
29. Khan SA; Siddiqui MF; Khan TA. Ultrasonic-assisted synthesis of polyacrylamide/bentonite hydrogel nanocomposite for the sequestration of lead and cadmium from aqueous phase: Equilibrium, kinetics and thermodynamic studies. Ultrasonics Sonochemistry. 2020;60:104761.
30. Bukhari A; Javed T; Haider MN. Adsorptive exclusion of crystal violet dye from wastewater by using fish scales as an adsorbent. Journal of Dispersion Science and Technology. 2023;44(11):2081-2092.
31. Haider MN. Enhanced Degradation of reactive violet 1 (RV1) Dye Using Gamma and UV Irradiation Coupled with Hydrogen Peroxide. Radiation Physics and Chemistry. 2025:113191.
32. Imran MS; Javed T; Areej I; Haider MN. Sequestration of crystal violet dye from wastewater using low-cost coconut husk as a potential adsorbent. Water Science and Technology. 2022;85(8):2295-2317.
33. Oukebdane K; Necer IL; Didi M. Binary comparative study adsorption of anionic and cationic azo-dyes on Fe_3O_4-bentonite magnetic nanocomposite: kinetics, equilibrium, mechanism and thermodynamic study. Silicon. 2022;14(15):9555-9568.
34. Parsaei A; Baezzat MR; Rahbar N. Metoprolol Removal from Water Using Fe_3O_4/TiO_2/Activated Carbon Nanocomposite: Adsorption Isotherm, Kinetics and Thermodynamics. Analytical and Bioanalytical Chemistry Research. 2022;9(3):281-291.
35. Rahman MM; Adhikary SR; Rabby MMR; Hassan MM; Knani S; Akhfer SH; Al Zuhanee MK. Production of functionalized clay-CNC based biopolymeric nanocomposite from agro-waste biomass for bulky industrial wastewater treatment via continuous column adsorption study with mathematical modeling: A critical review. Journal of Cleaner Production. 2025:145883.
36. Rahmani M; Dadvand Koohi A. Adsorption of malachite green on the modified montmorillonite/xanthan gum-sodium alginate hybrid nanocomposite. Polymer Bulletin. 2022;79(10):8241-8267.
37. Safarzadeh H; Peighambardoust SJ; Mousavi SH; Mohammadi R; Peighambardoust SH. Adsorption of methyl violet dye from wastewater using poly (methacrylic acid-co-acrylamide)/bentonite nanocomposite hydrogels. Journal of Polymer Research. 2022;29(4):113.
38. Abbasi A; Ahmad I; Ikram S. Exploration of adsorption efficiency mechanism and swelling behavior of novel green itaconic acid modified gellan gum hydrogel nanocomposite for the removal of noxious dyes. Journal of Polymers and the Environment. 2024;32(4):1684-1705.
39. Huang S; Li C; Cheng Z; Fan Y; Yang P; Zhang C; Yang K; Lin J. Magnetic Fe_3O_4@ mesoporous silica composites for drug delivery and bioadsorption. Journal of Colloid and Interface Science. 2012;376(1):312-321.
40. Sarker M; Song JY; Jhung SH. Adsorptive removal of anti-inflammatory drugs from water using graphene oxide/metal-organic framework composites. Chemical Engineering Journal. 2018;335:74-81.
41. Machado TS; Damin BIS; Marchezi G; Crestani L; Piccin JS. Advanced Composites for Drug Adsorption. Advanced Composites: Springer; 2023. p. 491-536.
42. Shekhar S; Sajitha E; Prasad V; Subramanyam S. High coercivity below percolation threshold in polymer nanocomposite. Journal of Applied Physics. 2008;104(8).
43. Yadav S; Asthana A; Chakraborty R; Jain B; Singh AK; Carabineiro SA; Susan MABH. Cationic dye removal using novel magnetic/activated charcoal/β-cyclodextrin/alginate polymer nanocomposite. Nanomaterials. 2020;10(1):170.
44. Sachit MA; Kareem SH. Isotherms and Thermodynamic Parameters of Metoprolol Drug Adsorption on the Prepared Mesoporous Silica. Baghdad Science Journal. 2024;21(3):1029-1029.
45. Moreno-Sader K; García-Padilla A; Realpe A; Acevedo-Morantes M; Soares JoB. Removal of heavy metal water pollutants (Co^{2+} and Ni^{2+}) using polyacrylamide/sodium montmorillonite (PAM/Na-MMT) nanocomposites. ACS omega. 2019;4(6):10834-10844.
46. Mohammadzadeh Pakdel P; Sayyar Z; Peighambardoust SJ. Remediation of basic dyes using Cloisite 30B embedded carboxymethyl cellulose grafted acrylic acid and itaconic acid nanocomposite hydrogela. Polymer Bulletin. 2024;81(15):13803-13824.
47. Melhi S; Algamdi M; Alqadami AA; Khan MA; Alosaimi EH. Fabrication of magnetically recyclable nanocomposite as an effective adsorbent for the removal of malachite green from water. Chemical Engineering Research and Design. 2022;177:843-854.
48. Massrour A; Peighambardoust SJ; Foroughi M; Foroutan R; Ramavandi B. Crystal violet removal by sodium alginate-g-polyacrylamide/hydroxyapatite/Cu-Fe LDH nanocomposite. Environmental Technology & Innovation. 2025;38:104149.
49. Malatji N; Makhado E; Ramohlola KE; Modibane KD; Maponya TC; Monama GR; Hato MJ. Synthesis and characterization of magnetic clay-based carboxymethyl cellulose-acrylic acid hydrogel nanocomposite for methylene blue dye removal from aqueous solution. Environmental Science and Pollution Research. 2020;27:44089-44105.
50. Malatji N; Makhado E; Modibane KD; Ramohlola KE; Maponya TC; Monama GR; Hato MJ. Removal of methylene

blue from wastewater using hydrogel nanocomposites: A review. Nanomaterials and Nanotechnology. 2021;11:18479804211039425.
51. Makhado E; Pandey S; Nomngongo PN; Ramontja J. Preparation and characterization of xanthan gum-cl-poly (acrylic acid)/o-MWCNTs hydrogel nanocomposite as highly effective re-usable adsorbent for removal of methylene blue from aqueous solutions. Journal of colloid and interface science. 2018;513:700-714.
52. Gurunathan S; Qasim M; Choi Y; Do JT; Park C; Hong K; Kim J-H; Song H. Antiviral potential of nanoparticles—can nanoparticles fight against coronaviruses? Nanomaterials. 2020;10(9):1645.
53. Mishra V; Bansal KK; Verma A; Yadav N; Thakur S; Sudhakar K; Rosenholm JM. Solid lipid nanoparticles: Emerging colloidal nano drug delivery systems. Pharmaceutics. 2018;10(4):191.
54. Wang Z; Zhang Z; He C; Wang Q. Advances in the application of hydrogel adhesives for wound closure and repair in abdominal digestive organs. Biomaterials Science. 2025;13(10):2606-2627.
55. Lee SH; Bajracharya R; Min JY; Han J-W; Park BJ; Han H-K. Strategic approaches for colon targeted drug delivery: an overview of recent advancements. Pharmaceutics. 2020;12(1):68.
56. Fredriksen BN. PLGA and PLA particles as vaccine delivery systems for Atlantic salmon: a study on formulation and use with an emphasis on immune responses. 2012.
57. Sharma S; Kaur J; Sharma G; Thakur KK; Chauhan GS; Chauhan K. Preparation and characterization of pH-responsive guar gum microspheres. International Journal of Biological Macromolecules. 2013;62:636-641.
58. Khudair ZJ; Kadam Z. Adsorption behavior of Chitosan-MWCNTS nanocomposite for the elimination of ofloxacin medication. Chem J Mold. 2024;19(1):84-92.
59. Kumar JA; Sathish S; Prabu D; Giri J; Makki E; Jayaprabakar J; Ziyayeva GK; Baigenzhenov O; Sathish T; Praveenkumar T. Waste shrimp shell mediated Chitosan-Magnesium Oxide nanocomposite: Synthesis, characterization and exploitation towards acenaphthene removal from aqueous solution. Alexandria Engineering Journal. 2024;104:124-135.
60. Khliwi FS; Alshamsi HA. Design of a Z-Scheme System with g-C_3N_4/WO_3/$ZnFe_2O_4$ Nanocomposite for Photocatalytic Degradation of Rhodamine B. Journal of Cluster Science. 2025;36(3).10.1007/s10876-025-02817-y.